Biomaterials Science

Accepted Manuscript

This article can be cited before page numbers have been issued, to do this please use: U. Daood, S. Aati, Z. Akram, J. Yeebee, C. Yongsze, A. Parolia, S. L. Lin and A. Fawzy, *Biomater. Sci.*, 2021, DOI: 10.1039/D1BM00555C.

ROYAL SOCIETY OF CHEMISTRY

rsc.li/biomaterials-science

View Article Online
DOI: 10.1039/D1BM00555C

ARTICLE

Characterization of Multiscale Interactions Between High Intensity Focused Ultrasound (HIFU) and Tooth Dentin: Effect on Matrix-Metalloproteinases, Bacterial Biofilms and Biological Properties

Received 00th January 20xx,
Accepted 00th January 20xx

DOI: 10.1039/x0xx00000x

Umer Daood[a]*, Sultan Aatib, Zohaib Akram[b], Joyce Yeea, Celine Yong[a], Abhishek Parolia[a], Liang Lin Seow[a], Amr S Fawzy[b]*

***Corresponding Authors: Dr Umer Daood**, Clinical Dentistry, Restorative Division, Faculty of Dentistry, International Medical University Kuala Lumpur, 126, Jalan Jalil Perkasa 19, Bukit Jalil, 57000 Bukit Jalil, Wilayah Persekutuan Kuala Lumpur, Malaysia.

***Dr Amr S Fawzy**, UWA Dental School, University of Western Australia, Nedlands, WA 6009, Australia; Email: amr.fawzy@uwa.edu.au

Email: amr.fawzy@uwa.edu.au (Tel: +61864572434); umerdaood@imu.edu.my (Tel: +601151664374)

To characterize multiscale interactions between high intensity focused ultrasound (HIFU) and dentin collagen and associated matrix-metalloproteinases; in addition, to analyse effect of HIFU on bacterial biofilms and biological properties. Dentin specimens were subjected to 5, 10 or 20 s HIFU. XPS-spectra were acquired and TEM performed on dentin slabs. Collagen orientation was performed using Raman spectroscopy. Calcium measurements in human dental pulpal cells (hDPCs) were carried out after 7 and 14 days. For macrophages, CD36+ and CD163 were analysed. Biofilms were analyzed using CLSM. Tandem Mass spectroscopy was performed for detection of hydroxyproline sequences along with human MMP-2 quantification. Phosphorous, calcium, and nitrogen were detected in HIFU specimens. TEM images demonstrated collagen network appearing fused together in HIFU 10 and 20 s specimens. Band associated with 960 cm^{-1} corresponds to stretching $\nu 1$ PO_4^{3-}. Control specimens showed intensive calcium staining followed by HIFU 20 s>HIFU 10 s>HIFU 5 s specimens. Macrophages in HIFU specimens co-expressed CD80+ and CD 163+ cells. CLSM images showed HIFU treatment inhibiting bacterial growth. SiteScore propensity determined effect of HIFU on binding site with higher DScore representing better site exposure on MMPs. Multiscale mapping of dentin collagen after HIFU treatment showed no deleterious alterations on the organic structure of dentin.

Key words: Tooth dentin; collagen; dentin bonding; high intensity focused ultrasound; MMPs; dentin related biofilms.

1.0. Introduction

The hierarchical structure of teeth is remarkable and organized displaying enviable mechanical properties [1]. Dentin is a composite tissue protecting the pulp from microbial attacks. It supports the highly mineralized enamel to withstand occlusal forces without fracture. Besides being a passive mechanical barrier, dentin plays a major role in defensive reactions for protection of the dentin-pulp complex [2]. The bulk of dentin contains the mineral phase, which constitutes ~ 70% by weight, followed by 20% organic material and 10% water [3]. The water content is not uniform throughout the structure of dentin, varying about 20-fold from deep to superficial dentin [4]. The organic phase consists of collagen fibrils and ground substance, while the inorganic phase consists of hydroxyapatite crystals [5]. Type I collagen

[a] *Clinical Dentistry, Restorative Division, Faculty of Dentistry, International Medical University Kuala Lumpur, 126, Jalan Jalil Perkasa 19, Bukit Jalil, 57000 Bukit Jalil, Wilayah Persekutuan Kuala Lumpur, Malaysia*
[b] *UWA Dental School, University of Western Australia, Nedlands, WA 6009, Australia*

View Article Online DOI: 10.1039/D1BM00555C

predominates as the major protein found in human dentin, constituting 90% of the organic matrix, although trace amounts (3%) of types III and V have been found [6]. The protein is formed as a result of self-assembly of a triple helix with coiled formation of the two α I and one α II chains [7]. Properties within the dentin tissue will vary according to the fibril orientation which is observed throughout the thickness of the tissue [8]. The collagen synthesis is invariably controlled by the odontoblasts. The pro-collagen chains are initiated in the rough endoplasmic reticulum [9]. Stable and durable dentin bonding is a direct result of adhesive resin fully encapsulating the demineralized collagen network forming the hybrid layer [10,11]. The adhesive interface is expected to have a permanent connection between the resin composite and dentin tissue [12]. However, the hybrid layer formed is not considered perfect due to the morphological, pathological, and physiological heterogeneity of the dentin structure [13]. There are adverse clinical consequences due to the hydrolytic degradation of the resin-dentin interface mainly by the MMPs. These enzymes degrade the extracellular matrix and collagen denaturing the triple-helical structure within the interface leading to consequences. Some of these consequences are marginal pigmentation, dentin hypersensitivity, and possible secondary caries. This inadvertently results in decreasing the longevity of the restorations [14]. Resin-dentin interface has been known to stay adhered even after 3-years of storage under in-vitro experimental conditions, contemplating strong interface bonding after application of degradation inhibitors [15]. Reis et al. [16] reported that the abundance of organic and water content within dentin is problematic for the hydrophobic monomers to infiltrate inside the demineralized dentin and renders successful dentin bonding, a challenge. Some of the other major obstacles in attaining a perfect hybrid layer are water penetration, complex interaction of the resin with collagen and limited degree of resin conversion [17,18].

The collagen Type-I triple helix domains have a primary structure with an amino acid sequence rich in hydroxyproline (HYP) and proline (Pro) in addition to glycines providing rigidity and stability [19]. The sequences have a pivotal role in the formation of stable crosslinks. The HYP/Pro ratio is considered as an indicator of Type I collagen changes which happen due to enzymatic processing of proline residue hydroxylation [20]. Based on this premise, these native crosslinks improve the tensile properties of dentin collagen [21] improving the resistance of collagen matrix against enzymatic degradation, a requirement prior to adhesive application [22]. These collagen fibers aid in anchoring composite resin restorations to the dentin substrate making them an important and significant factor for bond adhesion and its durability [23,24]. It is widely understood that bond durability can be increased by improving the mechanical properties of the dentin matrices protecting the collagen fibers [25].

One of the new approaches, using high intensity focused ultrasound therapy, has been acknowledged to produce various bioeffects. Much of our previous work has been focussed on ultrasonic energy to induce changes on dentin tissue for resin dentin bonding [26] and nanocrystal delivery [27]. A shock front is created as a result of non-linear acoustic effects producing a significant mechanical stress within biological tissues and coalescence of microcracks [28]. The micro bubbles created can erode or ablate tissues due to the liquefying effect [29] with generation of hydrodynamic pressure gradients, micro-streaming, and micro-jets [30]. The therapy with its non-invasive delivery of focused ultrasound energy leads to collagen contraction and remodelling [31] which may have implications on resin dentin bonding. In addition, the synergistic effect of HIFU exposure on remineralisation potential of dentin using hydroxyapatite treatment has been well established previously [27]. Research has shown that the micro-bubbles created can mechanically erode tissues by liquefying with a variable speed [32]. Moreover, HIFU has been successfully implemented as a possible alternative to current methods used in periodontal therapy to achieve smooth root surfaces [33] and delivering antibacterial nanoparticles into the dentinal tubules to enhance root canal disinfection [34]. With the ability of HIFU to alter surface characteristics, there is possible application in the field of dentistry. It can also be speculated that the cavitation effect can render collagen swelling on the substrate (dentin/bone) leading to irreversible changes. HIFU ablation is known to produce such effects on the collagen structures when used in other tissues [35]. These conclusions are largely based on the association of the HIFU effect with direct effect on collagen and hydroxyapatite ablation, with limited experimental demonstrations of how the effect would have made changes with the collagen matrix. The morphological appearance of collagen fibers shows a typical pattern of interlocking ribbon-like collagen fibers which protrude outwards from the dentinal surface due to the mechanical-removal of minimal inorganic surface with preservation of intact collagen surfaces [26]. A detailed evaluation of the application of the HIFU device for its effect on dentinal tissue and collagen was still unknown. Therefore, the aim of this pioneering study is to characterize the multiscale interactions between HIFU and dentin collagen Type I matrix and the associated intrinsic bound proteases (matrix metalloproteinases MMP-2 and 9). In addition, to investigate the effect of HIFU on dentin related bacterial biofilms and biological properties in term of macrophage analysis for cytotoxic assay for providing preliminary biosafety

information on the application of the device on mammalian cells [32].

2.0. Materials and Methods

Sound human molars (*n=130*) were collected (25–40 years) after ethical approval (grant#BDS I-01-2020(18) and RA/4/20/5863) was provided by the Institutional Review Boards. The teeth were cleaned and stored in 0.5% chloramine-T for 2 weeks at 4°C to be used within 1-month from extraction time. Dentin disc-shaped blocks/specimens (~3-mm) were cut from the mid-coronal dentin using diamond-blades under water coolant (Buehler, Lake Bluff, IL, USA). Pulp-spaces were cleaned from tissue remnant by excavation followed by saline irrigation. The exposed coronal dentin surfaces were wet polished with 600 grit-size SiC papers (5 mins) and sonicated for 15 min to remove cutting debris. Each dentin disc was divided into 4 equal quadrants and the quadrants (dentin specimens) were randomly distributed between the study groups to minimize the effect of dentin variations between the groups. All dentin disc shaped specimens were subjected to HIFU at different intervals.

2.1. HIFU Set-Up and Dentin Specimens Exposure to the Acoustic Fields

As adopted and modified from previous experimental HIFU protocols (26, 27, 33), the HIFU experimental set-up is schematically presented in Figure (1). Briefly, a bowl-shaped pre-calibrated HIFU piezo-electrical ceramic concave transducer (Model TQN20-20C30, Siansonic Technology Ltd, China) having 1 ±4% MHz frequency and Ø 20.2 internal diameter connected to a high frequency ultrasonic generator (MG30 megasonic generator, Siansonic Technology Ltd, China) was used in this study. Clear flat glass petri dishes (80 X 15 mm) were filled with degassed distilled water and stored at room temperature (20°C). After removing the cover of the water filled petri dish, HIFU concave transducer was placed and immersed in and continuous sinusoidal standard waveforms were generated creating a conical shaped stream of cavitation bubbles along the axis of the transducer with focal depth at 18.4 mm, focusing effect of the transducer. The maximum negative pressure at the focal point was approximately 10 bar as reconfirmed by a PVDF needle hydrophone, 184 mV/MPa over the 1 kHz −3 MHz, (RP-Acoustic, Germany) via hydrophone system connected to a TDS420 A digitizing oscilloscope (Tektronix, Beaverton, OR, USA) (26). The strongest ultrasonic pressure (about 10 bar) is measured at the focus where the stream is the narrowest. Each dentin specimen quadrant was positioned inside the water filled petri dish at the focal point of the immersed HIFU transducer as schematically presented in Figure (1). Dentin specimens were subjected to HIFU at three different exposure times: 5, 10 or 20 s. After HIFU exposure, specimens of all groups were retrieved from the petri-dishes and transferred separately to polystyrene containers for subsequent characterizations as detailed below.

2.2. Dentin XPS Analysis

XPS spectra were acquired using AXIS Ultra DLD electron spectrometer (Kratos, UK). Specimens were deployed with 180 W X-rays and Al Kα (1486.6 eV) monochrome. A survey spectrum comprising of 0–1200 eV was collected at a high-resolution spectra of C 1s, P 2p, and Ca 2p regions with a pass energy of 160 eV and 40 eV and data analysed using CasaXPS Software (Casa Software Ltd, United Kingdom).

2.3. TEM Analysis of Collagen

After HIFU exposure, dentin slabs were transferred in sterilized well plates. Control dentin slabs (*n=7/group*) obtained were etched with 10 wt% phosphoric acid for 15 secs in addition to the specimens which were treated with HIFU. The slabs were fixed, buffered using 0.1 M sodium cacodylate for 1h, and rinsed with distilled water. Specimens were dehydrated using ascending concentrations of ethanol and finally infiltrated with araldite resin. Ultrathin sections (~90nm) were prepared using ultra-microtome and a diamond knife with specimens collected on grids and eventually stained using uranyl-acetate, UO2(CH3COO)2·2H2O, for 10 min before TEM imaging at 100 KV (JEOL-1010, Japan).

2.4. Raman Analysis and Collagen Mapping

To obtain molecular insights in binding mode of collagen fibers, Schrödinger small-molecule drug discovery suite 2018-2 software was used. Structures of collagen Type I were downloaded from Research Collaboratory for Structural Bioinformatics Protein Data Bank (PDB) (http://www.pdb.org). Low energy conformations of all collagen molecules were docked and analyzed using binding site using extra precision (XP) mode which incorporates water desolation energy and protein-ligand structural motifs into binding free energy scoring function.

View Article Online
DOI: 10.1039/D1BM00555C

Collagen orientation mapping and bio-chemical analysis was performed using Raman spectroscopy (Horiba-Scientific Xplora, Villeneuve d'Ascq, France) with peaks identified on dentin discs (*n=10*) for v_1 v_3 phosphate vibration, with three sub-bands (1060, 1030 and 960 cm^{-1}). The v_4 PO_4 vibration was used at 552 and 604 cm^{-1} with hydroxyproline/proline and pyridinium ring vibration set at 850−870 cm^{-1} and 1032 cm^{-1} respectively. For single point analysis, the laser was focussed using AX100/0.90 NA air objective using a 600-lines/mm grating with the spectrometer equipped with CCD detector (DR-324B-FI-327, Andor Technology LTD, UK). There was a total of 50 scans performed per individual specimen over a 25 x 5.5 µm sample surface area with a maximum acquisition of 10 s. Fifth degree polynomial function was used for baseline correction. A near-infrared laser spot (diode; 0.5 $µm^2$) operated at 785 nm between 400-3200 cm^{-1} (100 mW sample surface power) were measured. Steps used to scan at different polarization angles include Δβ = 15◦, from β = 90◦ to β = −90◦. For calculation, the following equation was fitted in Matlab 7.5 (MathWorks Inc., Natick, MA, USA).

$$I = a(1 + b(\cos(2(\beta - c))))$$
(1)

2.5. Calcium Measurements

Explant outgrowth method was employed to prepare human dental pulpal cells (hDPCs) from extracted third molars. The cells were cultured in minimal essential medium supplemented with penicillin/streptomycin 50 mg/mL, amphotericin B 0.25 mg/mL, L-glutamine 2 mmol/L and 10% fetal bovine serum at 37oC in a 5% CO_2 atmosphere. The cells were expanded into 4 x dilution after fourth passage with cells reaching a confluency of 85%. These cells were incubated with a serum-free medium at sub confluence and later sub harvested for the following experiment. The cell lines were cultured in Dulbecco's Modified Eagle's Medium (DMEM, Sigma Aldrich, St. Louis, MO, USA) with 10% fetal bovine serum (FBS) and 1% penicillin/streptomycin (10,000 U/100 µg/mL) in a humidified incubator with 5% CO2 incubator at 37 ◦C. The cells were expanded into 4 x dilution after fourth passage with cells reaching a confluency of 85%. On the third day, the cells (3 x 10^4) were seeded on the pulpal side of the dentin discs (0.28 cm^2) inside 24-well plates and placed inside incubator r with 5% CO2 and 95% air at 37 ◦C. After HIFU treatment, dentin discs were washed with PBS and fixed using 4% paraformaldehyde for 5 mins and again washed for 5 minutes using PBS. Alazarin Red was added to the cell cultures and incubated for 10 mins. Later the discs were washed at least three times at day 7 and 14 to remove remaining Alazarin Red. Positive staining was evaluated using a light microscopy (LW 0.52 Nikon Japan, Eclipsee). For calcium quantification, Arsenazo III (40 mM in dH20) was used. The cells from each dentin disc were incubated overnight in lyses buffer (Tris pH 7.2, 150 mM NaCl, 1% Triton-X, 0.1% sodium dodecyl sulfate, 1 mM phenylmethylsulfonyl fluoride, 10 mM benzamidine, 2 lg/ml leupeptin) and kept in a rotating incubator. For calcium quantification, 100 µL of Arsenazo III was added to 50 µl of lysate and absorbance was measured at 650 nm using the SpectraMax 190 microplate reader (Molecular devices, Sunnyvale, CA, USA). The measurements were carried out in triplicates with a calcium standard run alongside experimental samples after 7 and 14 days.

2.6. Macrophages Analysis

Human peripheral blood mononuclear cell line, SC (CRL-9855 #LOT: 61834527) from our previous storage was used. At a concentration of 2 x 10^5 for one flask, Iscove's Modified Dulbecco's Media (IMDM; ATCC, Lot:63331110-Manassas/VA), 1 x 10^6 cells/mL were cultured supplemented with 0.05 mM 2-mercaptoethanol, 0.1 mM hypoxanthine, 0.016 mM thymidine and 10% FBS. The cells were cultured in 60ng/ml phorbol myristate acetate (PMA; Sigma P1585-Lot # SLBQ7454V) and lipopolysaccharide (LPS-PG Ultrapure/Porphyromonas gingivalis-TLR4 ligand; 0.1 µg/ml) placed over the macrophage cells added with interferon gamma (IFN γ-; 20ng/ml) with the M1 and M2 polarization procedure followed from Daood et al 2019. The cells were fixed using formalin and later treated with 10% goat serum and PBS. After exposure of HIFU with 5, 10 and 20 s in different specimen groups, cells were examined using CLSM (Fluoview FV 1000, Olympus, Tokyo, Japan) using light emission between 500-550 nm with an excitation wavelength of 488 nm and 10, 20 and 40X objective lens for direct observation. CD36+ and CD163 were analysed and no counter stains of nuclei were used for this experiment.

2.7. Microbiology

Experimental biofilms were grown on dentin discs (*n=10*) with a thickness of 2 mm. The specimens were polished with silicon carbide papers upto #2000 before the biofilm growth (±SD surface roughness 0.079±0.011 µm). S mutans test strain JCM 5705 was used ((RIKEN Bioresource Center, Wako, Japan) and grown anaerobically in brain-heart infusion broth using AneroPack™ (Mitsubishi Gas Chemical Company, Tokyo, Japan) at 37°C for 24±2h. The final concentration was adjusted to 10^8 CFU/mL. The dentin specimens were incubated with

600 µL of artificial saliva (prepared as per Hahnel et al 2008) in a 24-well plate for 2hrs at 37°C. After the required exposure, artificial saliva was removed, and the well plates were inoculated with the prepared bacterial suspension and grown anaerobically at 37°C for 24 hrs and plate shaken at 300 rpm (Micromixer E-36; TAITEC, Koshigaya, Japan).

Bacterial suspension from the cells were centrifuged (1ml of sterile distilled water) and placed on the bottom of the glass petri dish which was sealed tightly. The petri dishes were subject to HIFU treatments at different time points with each petri dish placed at the focal point generated by the transducer. For confocal examination, he Petri dish were stained with Film Tracer LIVE⁄DEAD Biofilm Viability kit (Life Technologies-Invitrogen, Grand Island, NY, USA). The specimens were incubated for 30 mins in the dark, excessive stain removed and analyzed with CLSM using light emission between 500 and 550 nm with an excitation wavelength of 488 nm and × 100 objective. The statistical results of biofilm quantification were obtained by micro-image analysis using Image J software. Impedance readings were taken at 15 min intervals for 48 hours after HIFU exposure in additional specimens (*n=5*) for each group and real-time cell index plotted on individual graphs in duplicates in every tested plate grown for another 2 days after HIFU exposure (data not shown).

2.8. Tandem mass spectroscopy

Twenty-five third molars were obtained and stored in sodium azide at 4°C after ultrasonic cleaning. After careful removal of roots, occlusal enamel was cut perpendicular to longitudinal axis of the tooth using isomet in IMU (Buehler, Lake Bluff, IL). A longitudinal furrow was made between the furcation area using a flexible diamond disc without touching the pulp tissue inside the pulp chamber. Pulp tissue was gently separated. The clean teeth segments were pulverized in liquid nitrogen into fine dentin powder using a steel mortar/pestle (Reimiller, Reggio Emilia, Italy). One gram of each dentin powder was divided into demineralised, HIFU experimental and control groups (no demineralization). Dentin powder was demineralised using 35% phosphoric acid for 15 seconds and rinsed for 20 s. For the HIFU specimens, 1 gram of dentin powder was placed inside petri dish attached to a metal support using cyanoacrylate adhesive. The petri dish was placed in water filled tank at the HIFU focal point and ultrasound energy generated at pre-determined exposure points of 5 s, 10 s and 20 s at an amplitude of 2 v and 250 kHz driven at a sinusoidal wave generating 120 v. Once done, specimens were retrieved and transferred separately to polystyrene containers to be stored.

Tandem Mass spectroscopy was performed at a resolution of minimum 60,000 for MS and MS/MS scans. Collision Induced Dissociation method (CID) was used for fragmentation of selected peptides. The Swiss Prot database with MASCOT search engine were used for annotation of MS/MS spectra. After fragment ion analysis and proline oxidation, the data was interpreted (addition of 16 Da to the mass of proline residue) as a modified parameter in MASCOT search engine for detection of Hyp PTM present in COLIIA1 peptide sequences.

2.9. MMPs Sequencing with heat maps and coding

Fluorescent peptides (China peptides; Shanghai) were dissolved in DMSO preparing 150 µg solutions. Stocks were prepared (100 µM) using molar coefficient of (2,4)-dinitrophenyl) 6.985 cm^{-1} mM^{-1} and DMSO at 400 nm. Purified pro-MMPs (MMP-2; British Biotech Pharma, Oxford, UK) were used to prepare aliquots of 10 µg and freeze with liquid nitrogen at -70°C and quenched peptide assays performed according to Daood et al 2020. Quantification for human MMP-2 was performed by Mascot version 2.2 (Matrix Science) and Tandem (2007.07.01). Searches were performed by analysing cleavage specificity and N-terminal set as variable modifications.

3.0. Results

Wide scan XPS analysis was performed for the control and HIFU treated specimens to determine the elements present on the dentin surfaces. The chemical composition of the surface of control dentin specimens and HIFU treated specimens revealed high percentages of carbon, oxygen, and phosphorus (Table 1). The elements phosphorous, calcium, and nitrogen were detected in all HIFU specimens (Figure 2A-B). Reduced levels of phosphorus (2.4), and calcium (2.1) were identified in 37% PA etched specimens ($p<0.012$). The HIFU group surfaces showed the same elements as those of the control groups (Table 1). The amounts of P2p were also similar between the control and HIFU treated specimens, other than the 37% etched demineralised dentin specimens, indicating more hydroxyapatite components. The carbon signal is also effectively identical in HIFU and control specimens in terms of intensity within the mineral.

The TEM images shown in Fig 2C present the 37% PA etched

demineralised dentin surface with collagen network appearing thinner along with presence of collagen gap channels (pattern appears random) showing undulating or wavy contour (Fig 2C). The fabric displays a random network of big collagen fibers. The highest possible packing is seen in (Fig 2D) 5, (Fig 2E) 10 and (Fig 2F) 20 s HIFU specimens. The white arrows indicate apatite crystallites aligned along the collagen axis in HIFU 20 s specimens (Fig 2G). Within the HIFU treated specimens, collagen fibrils were fused together showing typical stripes called D-period, which is the most typical feature observed under electron microscopy (* inset image Figure 2). Collagen fibrils are assembled by parallel arrays of collagen molecules with regularly longitudinal interlacing having a triple helix structure as seen in control specimens (Fig 3A-B). TEM images (Fig 3C) show area of aggregated and bundles of collagen in 5 s and (Fig 3D) 10 s HIFU specimens with clear D periodicity in (Fig 3E) HIFU 10 s and (Fig 3F) 20 s specimens. The white arrows depicted in Figure 3G indicate an overlap of collagen zones identified in the fibril at 5 nm supporting presence of intrafibrillar hydroxyapatite.

Using molecular simulation study, collagen Type I was identified within 5 Å with each of the identified lysine-arginine sites. The profile of bare collagen microstructure with water molecules is depicted in Figure 4A. The conformational change within the experimental structure spaces at macromolecular level with different molecules contributing to the flexible and dynamic structure is depicted. Periodic boundary conditions exploiting the D-band periodicity was used giving a replication of the dense fibrillar environment of the collagen matrix. This site is a likely place of intramolecular crosslink with its energy less than the energy of the reference module used during simulation shown in Figure 4A. In the single point Raman spectra (Fig 4B), the band associated with 960 cm^{-1} corresponds to the stretching v_1 PO_4^{3-} formed as a simultaneous contribution of surface and bulk phonons scattering from the hydroxyapatite crystals of the surface. This trend happened as the wavelength is enough to avoid the inelastic Raman scattering. The presence of hydroxyapatite can be compared between the specimens with symmetric phosphate stretching labelled as PO_4^{3-}; v_1. Phosphate Raman peaks were accentuated at 960 cm-1 in all HIFU and control groups. Along with the PO bands, proline bands were the most widely observed changes, a fingerprint region to investigate proteins (Fig 4B). Figure 4C reveals the oscillatory mean Amide I intensity of sinusoidal response of polarization θ angle of control and HIFU 5, 10 and 20 s treated specimens. This reflects degree of anisotropy which is increased in HIFU 20 s and control specimens. The orientation was determined using orientation of molecules in positions "a" and "b" (Fig 4C). Mapping was obtained using Amide I Raman band from different polarization angles corresponding to a full rotation $\phi = 0^0$ to $\phi = 180^0$. Collagen orientation map visualization of demineralized control (red curve) showed less anisotropy as compared to HIFU 20 s (green curve) and HIFU 10 s (golden curve) specimens. A similar feature of normal collagen fibrils was observed in the HIFU 20 s specimens (Fig 3D). The dentin specimens modified using HIFU 20 s showed fibrils interspersed between bundles of normal fibrils with a reduced contrast. They can be regarded as more mineralized and stable. This is primarily due to outer wrapping incrustation of minerals even after the ultrasound treatment (Fig 4C).

The presence of calcium in the cell cultures was confirmed using Alizarin Red staining (Fig. 5). The increase in cellular calcium concentration in the cultures over time was quantified using Arsenazo III (mmol/L). As shown in figure 5 A-B, there is a clear increase in the red nodules seen in the control specimens after 3 days. In general, all specimens cultured in the osteogenic media demonstrated intensive staining with control specimens showing the strongest control followed by HIFU 20 s (Fig 5H-I), HIFU 10 s (Fig 5F-G) and HIFU 5 s (Fig 5C-E) specimens (Fig 5). Using the data, there was a 30% increase in the amount of calcium within HIFU specimens as compared to the control (Table 1). HIFU 20 s specimens were most potent with the calcium concentration value of 39.8 mmol/L (25.9-50.0) after 7 days and 58.4 mmol/L (31.2-71.6) after 14 days with HIFU 10 s displaying 31.4 mmol/L and 44.8 mmol/L after 14 days, respectively. This was followed by 5 s specimens. HIFU 20 s specimens showed the maximum calcium increase compared to the control. Majority of macrophages in HIFU specimens co-expressed CD80+ and CD 163+ cells in variable intensities (Fig 6B-D) with M1 becoming dominant initially followed by a higher M2 profile within the HIFU specimens. These findings implied a difference in macrophages with a remarkable increase of M1 followed by M2 in HIFU specimens. Our findings suggested that macrophages from different HIFU treatments had a different propensity to produce M1 and M2 reactions, which are alternative reactions of the macrophages in response to the treatment offered.

The CLSM images of streptococcus mutans under and without HIFU treatment are shown in Figure 7. CLSM quantified the amounts of bacteria under HIFU treatment. The bacteria and the concomitant extra polysaccharide were labelled as green and red with respect to viability and death of microbial

colonies. The control specimens with no treatment displayed green densely clustered colonies with almost no areas of dead cells after 7 days (Fig 7A-B). CLSM images showed presence of HIFU treatment diminishing the growth of bacteria after 5 secs (Fig 7C). The 10 secs HIFU treated specimens appeared with dead bacterial colonies with no areas of surviving green stained bacteria, indicating no survivability (Fig 7D-E). The three-dimensional reconstruction of the S. mutans biofilms treated with 10 secs HIFU treatment was calculated as the ratio of EPS to S. mutans were performed with Imaris 8.0.0 (Fig 7F). The results were averaged from at least three randomly selected positions. The three-dimensional reconstruction of the S. mutans biofilms treated with 20 secs HIFU treatment also displayed complete dead microbial colonies (Fig 7H-I). The distributions of bacteria and EPS from each layer of the biofilms were also analyzed using COMSTAT (Fig 7J) demonstrating deproliferation of bacteria after HIFU 20 secs treatment.

The mass fingerprinting of the amino acid sequence (Fig 8A) with Swiss Prot database with MASCOT search engine were used for annotation of MS/MS spectra. The obtained fragments were ranging between 1000 and 3500 Dalton showing ~40% coverage in full length sequence of COLIIA1. Site specific hydroxyproline and proline derived from tryptic peptides of COLIIA1 for site specific characterization in between 1500 to 1800 Da peptides in all HIFU (20, 10 and 5 s) treated specimens annotated by fragmented ions at higher intensities (Fig 8A) were performed. The results of MMP-2 concentrations for HIFU 20 secs are depicted in Figure 8B. The P6-6' positions shown as black line are plotted amino acids identified between P1 and P1' with cleavage sites seen as heats maps show few amino acid occurrences within the peptide libraries (Fig 8B). There was a SiteScore propensity determining the effect of HIFU on the binding site with the higher DScore (data not shown) representing a better site exposure with the ligand being flexible and receptor was rigid (Fig 8C).

4.0. Discussion

High intensity ultrasound treatment has already shown promise for minimally invasive treatment of tooth substrate. Previous studies had introduced the proof-of-concept, interaction of high intensity focused ultrasound for resin dentin bonding, and its potential effect on root surface cementum as an alternative method of root planning, all with its technological limitations. In addition, the method displayed a favorable synergetic effect for a higher remineralization potential of demineralized dentin matrix following hydroxyapatite nanorod treatment [26 ,27 ,33]. The platform allows driving an interstitial probe development by combining previous results [26, 27, 33] and several research tools for clinical use. In this study, steps have been highlighted at a *multiscale* level to confirm HIFU in-vitro effects on dentin substrate. A relevant parameter in consideration when using the acoustic wave field is the pressure. In all experiments, except the biological cells, the energy was delivered directly for easier control. In case of the biological cells, an axial distance and presence of dentin disc between the acoustic energy and the cells has an experimental reasoning, as the energy does seem to be transmitted efficiently through the disc. In the procedure studied here, the HIFU treatment was proposed with encouraging results, while several aspects for probe development could be further studied using the developed platform, especially to optimize the future probe. Within the results of this study, the stated null hypothesis could be rejected as with HIFU exposure, there were differences on the substrate and sub-substrate level of dentin surface as reflected and confirmed from several characterization techniques employed. However, the energy penetration within the dentinal hard tissue could be affected by generation of the type of cavitation via the ultrasonic systems [36]. Moreover, these limitations can be due to the type of cavitation or the bubbles produced. By using HIFU under the parameter used in this study, the effect on the dentinal substrate may have been at the desired depths. Since the methodology is reflected at tooth surface between the substrate and the device, the presence of tooth surface in front of the device clinically can be problematic. Sonication through the dentinal surface can be particularly challenging owing to variable thickness and density of different teeth structures. Therefore, an appropriate "acoustic window" may be required for an ultrasound beam to propagate to the target. In addition to this, clinically relevant target volumes maybe very large, although the results were applicable and positive towards a better substrate stability. Therefore, design and testing of a HIFU system with flexible and controllable multi focus pattern ability is another important advance that the authors need to investigate. The transducer used has allowed increased effects to enhance inorganic tissue removal thus achieving reduced treatment times – and research in this area is ongoing. However, all these effects need to be further studied and investigated in future experiments.

XPS analysis confirmed that hydroxyapatite remained substantially on the dentin surface after HIFU treatment with phosphorous, calcium, and nitrogen detected. Low levels of

phosphorus (2.4) and calcium (2.1) were identified in 37% PA etched specimens ($p<0.012$). Both elements, phosphorous and calcium were found in conjunction with the dentin organic substance as shifts in these peaks are due to differences in HIFU treatment. Our results indicated a shift of approximately 1 eV lower after treatment of specimens with 10 and 20 s. The intensity of phosphorous signal showed integration area of phosphorus peaks at 187.58 eV. It is speculated that phosphate group may have formed hydrogen bonds with the substrate collagen lowering the bonding energy to 1 eV. The interaction of HIFU on mineralised dentin was reported previously [27] with prolonged exposures (60-120s) as there were minimal adverse effects noted on the structural integrity of collagen fibers. Shorter HIFU exposure times [5-20 s] were employed in this study to preserve the integrity further. There was structural integrity and conformational stability of dentin-collagen fibrils in HIFU specimens shown by TEM images (Figures 2, 3 and 4) which might be attributed to reduced destruction of minerals protecting collagen fibrils and the associated changes in orientation of tropocollagen molecules [37] leading to a denser and close to normal collagen-matrix and associated D-banding. It is reported that HIFU focused ultrasound waves using a focusing transducer show minimal damage to surrounding tissues that is primarily due to the formation cavitation bubbles [38]. There is a non-equilibrium oscillation state formed because of kinetic energy being released after collapsing due to high-speed jets [39].

Dentin-matrix with high collagen fibrillar integrity is more efficient for neutralizing acidic biofilm effects and is more liable to efficient remineralization process [40]. The banded structure observed in 10 s (Fig 2E) and 20 s HIFU specimens (Fig 2F) indicates an array of overlap gap zones of a normal collagen structure with clearly visible light and dark alternate bands. All HIFU specimens showed similar banding patterns referring to collagen periodicity at 69.0 nm and 65.6 nm [41]. Phosphoric acid specimens showed typical patterns of demineralisation with thinner collagen fibrils morphologically different from HIFU treated specimens which had inorganic-minerals aligned and associated with the collagen-fibrils and inter-fibril spaces (Fig 2C). No damage (Fig 3E-G) is expected around the focused area as the ultrasound energy is of lower acoustic energy and adverse effects are rare [42]. This preservation of collagen is critical for the potential application of HIFU technology as an alternative to dentin acid etching. Moreover, HIFU generates heat enabling collagen to form bridging bonds [43] to other collagen fibers (3C-D) which may be due to physically adjacent collagen and ordered formation [44] forming protein aggregates. Temperature was monitored using a digital thermometer (Iso-Tech IDM 207, Northants, UK) showing that the temperature of the culture medium only marginally increased by 0.4^{o}C after the HIFU treatment in real time. Although the temperature regulation at the focal point during HIFU treatment is critical, our previous studies focused on dentin treatment monitored during HIFU treatment with temperature sensors showing no adverse changes. The average value and standard deviation of the temperature variation from the room temperature of water before HIFU exposure was measured at different time points. It was concluded that the thermal stress within the experimental set up was negligible. The control group used was not exposed to the HIFU experimental treatment or factor to compare the results between the experimental HIFU groups and demineralised control groups. The non-use of non-demineralised samples as the control was logical, as the non-demineralised specimens were expected to display no difference in outcome or appearance of organic structure due to no demineralisation experimental treatment, especially when the XPS results demonstrated no changes within the inorganic structure. The main comparison was between the collagen exposure seen between the demineralising 37% phosphoric acid procedure and HIFU. So, the demineralised control specimens used were particularly useful for validating the experimental procedure.

Raman analysis indicated a strong interaction between organised maturation of apatite lattice and mineral maturity at the collagen-mineral interface of HIFU treated specimens (Fig 4B). This has a major contribution on the quantity of electrostatic bonds between the collagen matrix and the minerals [45]. The Raman fitting method was an alteration between the modulation of mean intensity and change in collagen orientation with increased angles. Raman peaks at 960 cm^{-1} indicate a higher hydroxyapatite for specimens treated with HIFU 10- and 20 s showing the highest spectrum supporting the analogy that dentin-collagen matrix has more mineralised matrix. The oscillatory mean Amide-I intensity gives a precise sinusoidal response of polarization angle β (Fig 4C) reflecting much anisotropy. HIFU 10 and 20 s specimens showed increased anisotropy in positions 'a' and 'b' as compared to control specimens. There was a full rotation ϕ – 0o to ϕ = 180o while doing the mapping at different angles of polarization with demineralised control specimens showing less anisotropy (red curve) as compared to HIFU 20 s specimens (green curve). There is an increase in CN-band intensity and a decrease in NH-plane. Site specific

View Article Online
DOI: 10.1039/D1BM00555C

hydroxyproline and proline derived from tryptic peptides of COLIIA1 for site specific characterization in between 1500 to 1800 Da peptides in all HIFU treated specimens annotated by fragmented ions at higher intensities. This presence of proline and hydroxyproline contributed towards formation of planar peptide bonds within the matrix structure of dentin, strongly suggesting a triplet structure in collagen α chain space [46] with stabilization of triple helix structure.

No detrimental effect on mineralised nodule production was observed in HIFU 10 and 20 s specimens. However, this conclusion can be further confirmed and verified in vivo before a conclusion can be drawn. The normal deposition of nodules after HIFU treatment indicates that reparative processes were minimally affected. Notably HIFU treatment enhanced nodule formation in the cell culture (Fig 5H-I). Several studies have shown that ultrasound simulation leads to increased protein [47] and collagen synthesis [48]. The expression of mineralized nodules indicates high activity in mineralized tissues [49]. This normal deposition of mineralized nodules is a strong indication that dentin pulp reparative processes can function without any detrimental issues, which is pivotal for tertiary dentin formation. We speculated that the HIFU probably promoted the nodule formation. However, this speculation needs to be verified, and further studies are necessary to clarify how HIFU activates the hDPCs before rendering it absolute safe for use in association with dentin bonding.

Few results associated with the current study are worth mentioning. The HIFU effects are a result of two main mechanisms namely the thermal and non-thermal pathways through acoustic-cavitation, radiation-pressure, and acoustic-streaming [50]. They generate shock waves causing localised and controlled tissue changes [51] depended on exposure times and focussed intensities. HIFU treatment at different time exposures shifts the macrophage polarisation phenotypically from M1 to M2 macrophage polarization and thereby triggering CD163, and CD36, suggestive of tissue healing [52]. The results showed inflammatory macrophages were present after HIFU 10 and 20 s treatment (Fig 6C-D) indicating the influence of HIFU on polarization of macrophages. The results are similar to a previous study done by Sukubo et al in which they demonstrated the use of shock waves against macrophages culture where low energy shock waves increased the expression of anti-inflammation resident macrophage marker genes. The macrophage phenotypes are much more diverse, overlapping each other in function revealing many hybrid states forming a continuum of activation states [53] depending on the HIFU treatment.

The ability of high-powered ultrasound to damage and disrupt biological cell walls is also pivotal in understanding the effects on microbes. However, a complete removal of bacterial colonies via HIFU alone might not be enough. Therefore, HIFU can be used in combination with other techniques such as use of cavity disinfectants [54]. Moreover, the CLSM images confirmed the ability of HIFU 20 s to kill *S. mutan* colonies (Fig 7G) attached on the tooth substrate. The ultrasound effect may have killed and redistributed the biofilm bacteria all over the dentin surface so that all dead cells were seen on CLSM images at different locations or may have been dislodged. Two thresh holds were identified at 10 and 20 s that were not significantly different from each other ($p<0.05$). After balancing the factors of exposure time and biofilm eradication efficacy, the exposure time of 20 s was viewed as our optimal exposure time. Furthermore, the inertial cavitation produced during HIFU produces shear via bubble collapse or bubble expansion/ jetting on bacteria or shock waves [55-56]. The cavitation may have also disrupted the bacterial walls inactivating bacteria by rupturing of bubbles due to vibrations of shock waves focused on a small area. Ultrasound activation creates pores inside cell walls causing irreparable damage to bacteria [57].

The results of MMP-2 concentrations for HIFU 20 secs are depicted in Figure 8B. There was a SiteScore propensity determining the effect of HIFU on the binding site with the higher DScore (data not shown) representing a better site exposure with the ligand being flexible and receptor was rigid (Fig 8C). The MMP profile scores based on P1 positions with respect to Glu residues shows adequate scores in HIFU treated specimens. In quantitative proteomics, there are multiple proteins quantification but are finally averaged determining the abundance of protein to correlate the analysis with direct MMPs and cathepsin-k analysis [58]. MMP-2 active site mapping with heat map for amino acid occurrences at P', P3 proline and P1' positions identified adding further endorsement to the (C) cleavage sites being tested for MMP-2. The effect of MMPs and cathepsins on dentin bond degradation are of significant importance [59].

High intensity focused ultrasound can be beamed at specified treatment sites to induce control change and volume reduction without much damage to the substrate, which in this case is dentin. Any form of dentin damage is counterintuitive, the change brought about can bring a change within the collagen structure, such as contraction [31]

View Article Online
DOI: 10.1039/D1BM00555C

which may display its effects on resin-dentin bonding. To achieve localized biological effects, HIFU transducers in our study were designed with geometric focusing such that ultrasound beams were focused to converge at a focal point. This takes advantage of the spherically/cylindrically concave surface of HIFU transducers that causes ultrasound waves to arrive at a focal point. The cavitation caused by this methodology is a kind of histotripsy based HIFU effect in which short repeated HIFU pulses cause rapid oscillation of microbubbles and break down the substrate (inorganic dentinal layer) without significant heating. The non-ionizing nature of HIFU eliminates radiation risks and allows for repeating therapy as needed without dose limitations. Induced biological effects are localized at the focal point without significant effects at the near or far fields [60] as seen in the current study. Also, in our study, we were able to measure temperature in the focus of HIFU during stimulation. We did not find any significant temperature elevation, even when using prolonged stimulation of 20 s.

A minimization technique was deployed that ensured a good compromise between the target dentinal surface and position of the HIFU. The results within the study enabled us to reject the null hypothesis. The HIFU technology, with all its benefits can be of potential significance in adhesive/restorative dentistry owing to its localised alteration capabilities and biofilm effect [61]. HIFU provides a less invasive approach and is generally safe and can be clinically effective to have a potential clinical acceptance in modern adhesive dentistry. However, this technology in dentistry is still in its infancy and further studies are required for technical considerations and making it possible to be used in a dental clinical set up.

Conclusions

Multiscale mapping of dentin collagen after HIFU treatment showed no deleterious alterations on the organic structure of dentin. The proposed timed protocols were suggestive of minimal damage to dentin structure with optimum mineralisation and stable organic structure, supportive for a non-deteriorating resin-dentin bond, implicated for future studies. These current results are promising for the efficacy of procedures with microbial burdens. The effects of HIFU therapy on dentin prior to bonding are still a challenge to researchers; increased knowledge about the effects on tooth tissues is important in the treatment of different clinical conditions.

Author Contributions

Amr Fawzy- Conceptualization, Methodology, Funding acquisition, Writing- original draft; Sultan Aati - Data curation, Writing- original draft; Zohaib Akram - Resources, Project administration; Joyce Yee, Celine Yong - Investigation, Project administration; Abhishek Parolia, Liang Lin Seow- project administration, editing; Umer Daood- Validation, Writing original draft, Reviewing and Editing, Methodology, Funding acquisition

Conflicts of interest

The authors declare no conflict of interest. The funders had no role in the design of the study; in the collection, analyses, or interpretation of data; in the writing of the manuscript, or in the decision to publish the results.

Acknowledgements

The authors thank the labs at Mimos Research Center, School of Dentistry of the International Medical University Kuala Lumpur, Centre of Bioactive Molecules & Drug Delivery, Institute for Research, Development & Innovation, International Medical University, and UWA Dental School Biomaterials Lab for the research experiments and analysis. This work was supported in part by Australian National Health Medical Research Council (NHMRC) Idea Grant (1188401-RA/1/3330/83), International Medical University, School of Dentistry #BDS I-01-2020(18) and Ministry of Health Malaysia FRGS/1/2020/SKK0/IMU/02/10 Project. The authors would also thank Ms Rebecca for her assistance in cell culture work.

Ethics approval

The human ethical committee at International Medical University Kuala Lumpur, approved the study bearing the protocol number (IMU R 259/2020).

References

1. A. Singhal, A.C. Deymier-Black, J.D. Almer and D.C. *Mater. Sci. Eng. C. Mater. Biol. Appl*. 2013, 33, 1467–75.
2. L. Tjaderhane, M.R. Carrilho, L. Breschi, F.R. Tay, D.H. Pashley. Dentin basic structure and composition—an overview; John Wiley & Sons A/S. Endo Top. 2012;20:3-29.
3. D.H. Pashley. *Crit. Rev. Oral. Biol. Med.* 1996, 7, 04-133.
4. M.C. Dean. Incremental markings in enamel and dentine: what they can tell us about the way teeth grow. In: Teaford MF, Smith MM, Feguson MWJ. Development, Function and Evolution of Teeth. Cambridge, Cambridge University Press.;2000.119-130.
5. A. Linde and M. Goldberg. *Crit. Rev. Oral. Biol. Med.* 1993, 4, 679-728.

6. A. Marten, P. Fratzl, O. Paris and P. Zaslansky. *Biomater.* 2010, 31, 5479-5490.
7. M.H.M. Wassen, J. Lammens, J.M. Tekoppele, R.J.B. Sakkers, Z. Liu, A.J. Verbout and E.A. Bank. *J. Bone. Miner. Res.* 2000, 15, 1776-1785.
8. J.H. Kinney, J.A. Pople, G.W. Marshall and S.J. Marshall. *Calcif. Tissue. Int.* 2001, 69, 31-37.
9. T.J. Wess. *Adv. Protein. Chem.* 2005, 70, 341-374.
10. N. Nakabayashi, M. Ashizawa and M. Nakamura. *Quintessence. Int.* 1992, 23, 135-141.
11. D.H. Pashley, F.R. Tay, L. Breschi, L. Tjäderhane, R.M. Carvalho, M. Carrilho and A. Tezvergil-Mutluay. *Dent. Mater.* 2011, 27, 1-16.
12. L. Tjäderhane. *Oper. Dent.* 2015, 40, 4-18.
13. L, Tjäderhane, M.R. Carrilho, L. Breschi, F.R. Tay and D.H. Pashley. *Endo. Top.* 2012, 4, 3-29.
14. S. Kermanshahi, J.P. Santerre, D.G. Cvitkovitch, and Y. Finer. *J. Dent. Res.* 2010, 9, 996– 1001.
15. U. Daood, K.S. Hanan Abdel, J.K.H Tsoi, and A.S. Fawzy. Int. J. Adhe. Adhes. 85, 2018, 263-273.
16. A. Reis, A.D. Loguereio, R.M. Carvalho and R.H. Grande. *Dent. Mater.* 2004, 7, 669-676.
17. N. Nakabayashi, K. Kojima and E. Masuhara. *J. Biomed. Mater. Res.* 1982, 3, 265-273.
18. L. Breschi, A. Mazzoni, A. Ruggeri, M. Cadenaro, R. Di Lenarda and E. De Stefano Dorigo. *Dent. Mater.* 2008, 1, 90-101.
19. K. Kadler. *Protein. Profile.* 1995, 2, 508–523.
20. U. Daood, Z. Akram, J.P. Matinlinna and A.S. Fawzy. *Dent. Mater.* 2019, 7, 1017-1030.
21. A.K. Bedran-Russo, G.F. Pauli, S.N. Chen, J. McAlpine, C.S. Castellan, R.S. Phansalkar, T.R. Aguiar, C.M. Vidal, J.G. Napotilano, J.W. Nam and A.A. Leme. *Dent. Mater.* 2014, 1, 62.
22. A.K. Bedran-Russo, P.N. Pereira, W.R. Duarte, J.L. Drummond and M. Yamauchi. *J. Biomed. Mater. Res. Part. B. Appl. Biomater.* 2007, 1, 268.
23. A. Frassetto, L. Breschi, G. Turco, G. Marchesi, R. Di Lenarda and F.R. Tay. *Dent. Mater.* 2016, 3, 1175–1187.
24. L. Tjäderhane, F.D. Nascimento, L. Breschi, A. Mazzoni, I.L. Tersariol and S. Geraldeli. *Dent. Mater.* 2013, 10, 999–1011.
25. C.M.P. Vidal, T.R. Aguiar, R. Phansalkar, J.B. McAlpine, J.G. Napolitano and S.N. Chen. *Acta. Biomater.* 2014, 7, 3288–3294.
26. A.S. Fawzy, U. Daood and J.P. Matinlinna. *Dent. Mater.* 2019, 7, 979–989.
27. U. Daood and A.S. Fawzy. *Dent. Mater.* 2020, 3, 456-467.
28. O.A. Sapozhnikov and M.R. Bailey. *J. Acoustic. Soc. Am.* 2013, 2, 661–676.
29. A. Maxwell, O. Sapozhnikov, M. Bailey, L. Crum, X. Zhen, B. Fowlkes. *Acoust. Today.* 2012, 11, 824–37.
30. S. Arrojo, Y.A. Benito. *Ultrason. Sonochem.* 2008, 1, 203–211.
31. R.W. Brobst, M. Ferguson and S.W. Perkins. *Facial. Plast. Surg. Clin. North. Am.* 2012, 2, 163-176.
32. International Organization for Standardization. Biological evaluation of medical devices-part 5: tests for in-vitro cytotoxicity ISO-10993-5; 2009 (en). 3rd ed. International *Organization for Standardization; 2009.*
33. U. Daood and A.S. Fawzy. *Arch. Oral. Biol. 2018, 2, 195-203.*
34. A. Shrestha, S.W. Fong, B.C. Khoo, A. K. *J Endo*. 2009, 7, 1028-1033.
35. F. Jiang, M. He, Y.J. Liu, Z.B. Wang, L. Zhang, J. Bai. Ultrason, 2013, 53, 77-83.
36. P. Sequeira, Z. Fedorowicz and M. Nasser. *Cochrane. Database. Syst. Rev. 2007, 17, CD006384.*
37. F. Ortolani and M. *Marchini.* Boll. Soc. Ital. Biol. Sper. *1993, 1,* 49-*55.*
38. S.C. Lea, G.J. Price and A.D. Walmsley. *Ultrason. Sonochem. 2005, 3, 233-236.*
39. K.S.F. Lew, E. Klaseboer and B.C. Khoo. *Sens. Actuator. A. Phys. 2007, 1, 161-172.*
40. R. Osorio, E. Osorio, A. Medina-Castillo and M. Toledano. *J. Dent. Res.* 2014, 12, 1258.
41. J.P.R.P. Orgel, T.C. Irving, A. Miller and T.J. Wess. *Proc. Natl. Acad. Sci. USA.* 2006, 24, 9001-9005.
42. M.R.D. Brown, P. Farquhar-Smith, J.E. Williams, G. ter Haar and N.M. deSouza. *Br. J. Anaesth.* 2015, 4, 520-530.
43. R.W. Martin, S. Vaezy, P. Kaczkowksi, G. Keilman, S. Carter and M. Caps. *Ultra. Med.* 1999, 6, 985.
44. A. Tokarczyk, I. Rivens, E. van Bravel, R. Symonds-Tayler and G. ter Haar. *Phys. Med. Biol.* 2013, 15, 2281.
45. D. Farlay, G. Panczer, C. Rey, P. Delmas and G. Boivin. *J. Bone. Miner. Metab.* 2010, 4, 433-445.
46. H. Cao and S.Y. Xu. *Food. Chem.* 2008, 2, 439-445.
47. D.F. Webster, J.B. Pond, M. Dyson and W. Harvey. *Ultra. Medi. Bio.* 1978, 4, 343-351.
48. D.F. Webster, W. Harvey, M. Dyson and J.B. Pond. *Ultrason.* 1980, 1, 33-37.
49. E.E. Golub and K. Boesze-Battaglia. *Curr. Opin. Orthop.* 2007, 5, 444–448.
50. V.F. Humphrey. *Prog. Biophys. Mol. Bio.* 2007, 1-3, 195-211.
51. P. Delphine, K. Lew, E. Klaseboer and B.C. Khoo. *Phys. Fl.* 2009, 8, 083304.
52. F.O. Martinez, A. Sica, A. Mantovani and M. Locati. *Front. Biosci.* 2008, 13, 453-461.
53. N.G. Sukubo, E. Tibalt, S. Respizzi, M. Locati and M.C. d'Agostino. *Int. J. Surg.* 2015, Pt-B, 124-130.
54. U. Daood, M.F. Burrow, and C. Yiu. *Clin. Oral. Invest.* 2020, 2, 649-661.
55. Z. Xu, J.B. Fowlkes and E.D. Rothman. *J. Acoust. Soc. Am.* 2005, 1, 424-435.
56. C.M.C. Tempany, N.J. Mcdannold and K. Hynynen. *Radio.* 2011, 1, 39-56.
57. X. Shuang, C. Hua, L. Jianhu, A. Vishnu Prasad, Y. Min, D. Yu, L. Dairong and D. Yonghong. *Int. J. Hyper.* 2019, 1, 885-895.
58. U. Eckhard, P.F. Huesgen, O. Schilling, C.L. Bellac, G.S. Butler, J.H. Cox, A. Dufour, V. Goebeler, R. Kappelhoff and U. auf dem Keller. *Matrix Biol.* 2016, 2, 37-60.
59. Y. Liu, L. Tjäderhane, L. Breschi, A. Mazzoni, N. Li, J. Mao, D.H. Pashley, and F. Tay. *J Dent Res.* 2011, 8, 953968.
60. A.D. Maxwell, C.A. Cain, A.P. Duryea, L. Yuan, H.S. Gurm, Z. Xu. *Ultra. Med. Biol.* 2009, 35, 1982—1994.
61. K. Iqbal, S.W. Ohl, B.C. Khoo, J. Neo and A.S. Fawzy. *Ultra. Med Biol.* 2013, 5, 825– 833.

View Article Online
DOI: 10.1039/D1BM00555C

Table 1: Summary of data obtained from XPS measurements of dentin samples and location-matched along with alizarin red calcium concentrations of different specimens after 7 and 14 days.

Groups	Element	Measurements (2–4 spots per sample)	Average atomic%/ 100%	Standard deviation	(p<0.05)	Ca^{++} (7 days) mmol/L	Ca^{++} (14 days) mmol/L
Control (α)	Phosphorus (P2p)	52	3.8	1.4	0.012*	6.7 (3.4-7.9)	27.2 (11.1-44.1)
	Carbon (C1s)	51	61.2	13.3			
	Calcium (Ca2p)	51	4.9	1.1			
	Nitrogen (N1s)	51	4.5	1.9			
	Oxygen (O1s)	51	23.6	5.9			
Control 37% PA (β)	Phosphorus (P2p)	41	2.4	0.8	≤0.04	5.1 (2.2-8.1)	17.7 (7.1-[illegible])
	Carbon (C1s)	37	45.6	11.2			
	Calcium (Ca2p)	39	2.1	0.6			
	Nitrogen (N1s)	22	3.3	0.8			
	Oxygen (O1s)	44	15.1	4.1			
5 sec HIFU (ϕ)	Phosphorus (P2p)	50	3.5	1.7	≤0.03	8.8 (5.3-15.1)	23.2 (9.1-[illegible])
	Carbon (C1s)	49	51.7	13.1			
	Calcium (Ca2p)	48	7.8	0.9			
	Nitrogen (N1s)	49	4.1	1.2			
	Oxygen (O1s)	49	18.8	5.1			
10 sec HIFU (δ)	Phosphorus (P2p)	47	3.9	1.1	≤0.05	31.4 (18.7-51.4)	44.8 (29.[illegible]-59.8)
	Carbon (C1s)	46	45.7	9.1			
	Calcium (Ca2p)	47	4.1	1.0			
	Nitrogen (N1s)	47	2.9	1.6			
	Oxygen (O1s)	50	13.1	3.6			
20 sec HIFU (∞)	Phosphorus (P2p)	45	3.7	0.5	≤0.06	39.8 (25.9-50.0)	58.4 (31.[illegible]-71.6)
	Carbon (C1s)	41	38.1	4.1			
	Calcium (Ca2p)	47	3.1	0.3			
	Nitrogen (N1s)	48	2.0	0.5			
	Oxygen (O1s)	47	9.9	1.1			

View Article Online
DOI: 10.1039/D1BM00555C

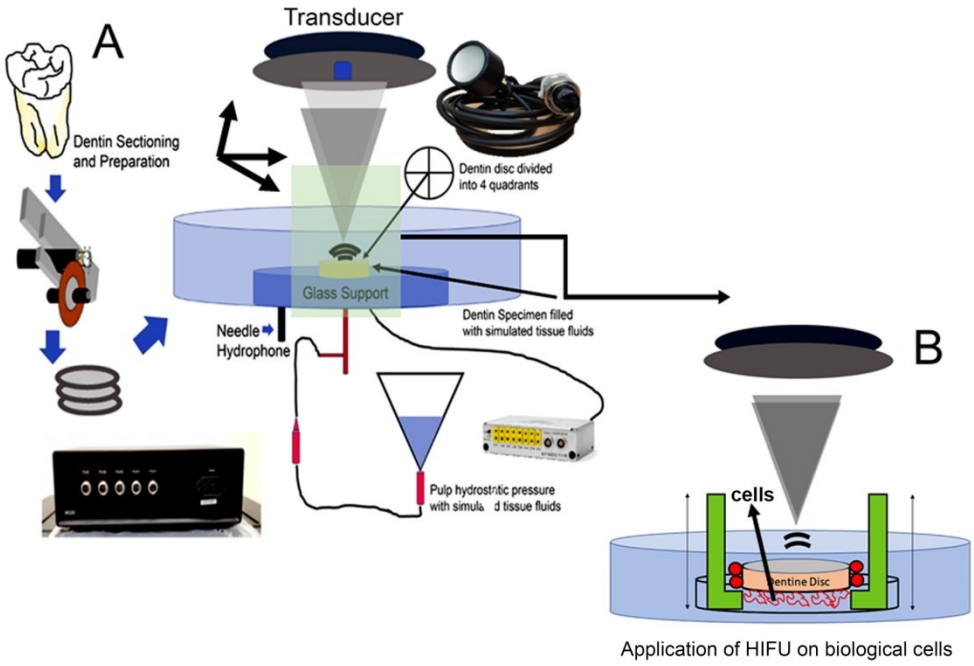

Schematic diagram of the HIFU system setup for application of treatment on dentin specimens. (A) The HIFU transducer was held approximately perpendicular to the dentin specimens (XYZ stage). The circle indicates the approximate location of the HIFU focus as per quadrant on dentin specimens. The grey arrows show upstream and downstream points that are the same distance from the sonicated location; (B) For application of HIFU on macrophages and hDPCs, the focused ultrasound beam passes through the overlying dentin specimen without a direct interaction towards cells which are lying deeper to dentin simulating the clinical relevance.

177x127mm (300 x 300 DPI)

View Article Online
DOI: 10.1039/D1BM00555C

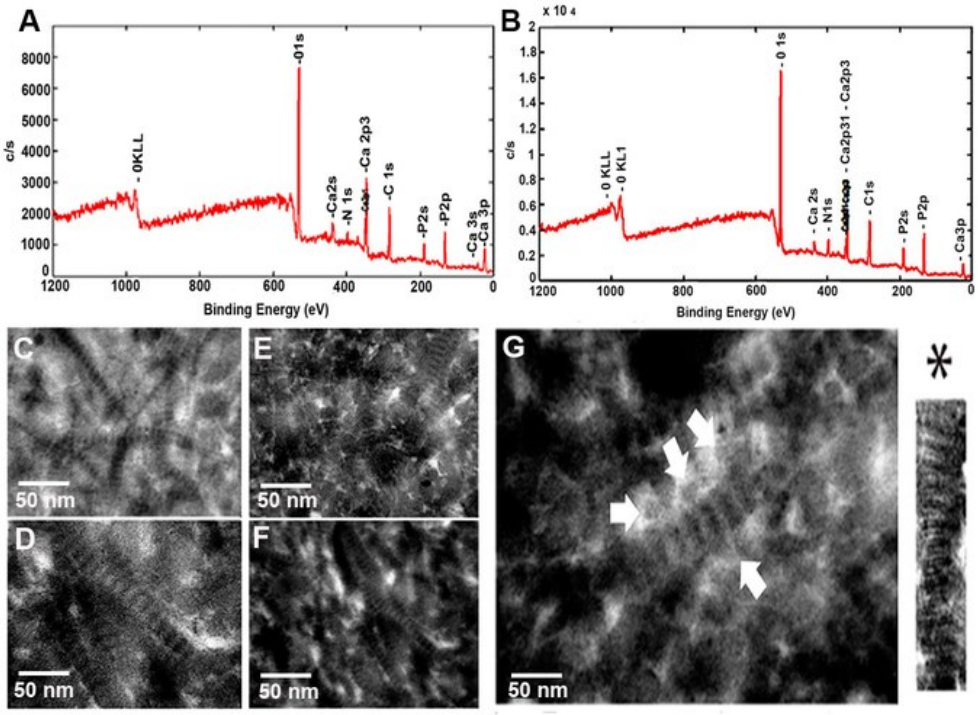

Representative raw XPS spectrum of dentin (A) control and (B) HIFU 20 s specimens, showing peaks where X-ray energy is enough for detection. Wide-scan XPS data depicts C, N, O, P and Ca. The HIFU 20 s group surfaces showed the same elements as those of the control groups. TEM images of collagen fibers with fibrous aggregates with light and dark streak features (D-period) can be seen in fibers in all specimens. The collagen network appeared thinner within the (C) 37% PA etching specimens with collagen gap channels (pattern appears random). The highest possible packing is seen in (D) 5, (E) 10 and (F) 20 s HIFU specimens. (G) The white arrows indicated apatite crystallites aligned along the collagen axis in HIFU 20 s specimens: * single and averaged image from unstained uranyl acetate TEM image showing positive bands indicating the positions of N- and C-telopeptides.

58x42mm (300 x 300 DPI)

View Article Online
DOI: 10.1039/D1BM00555C

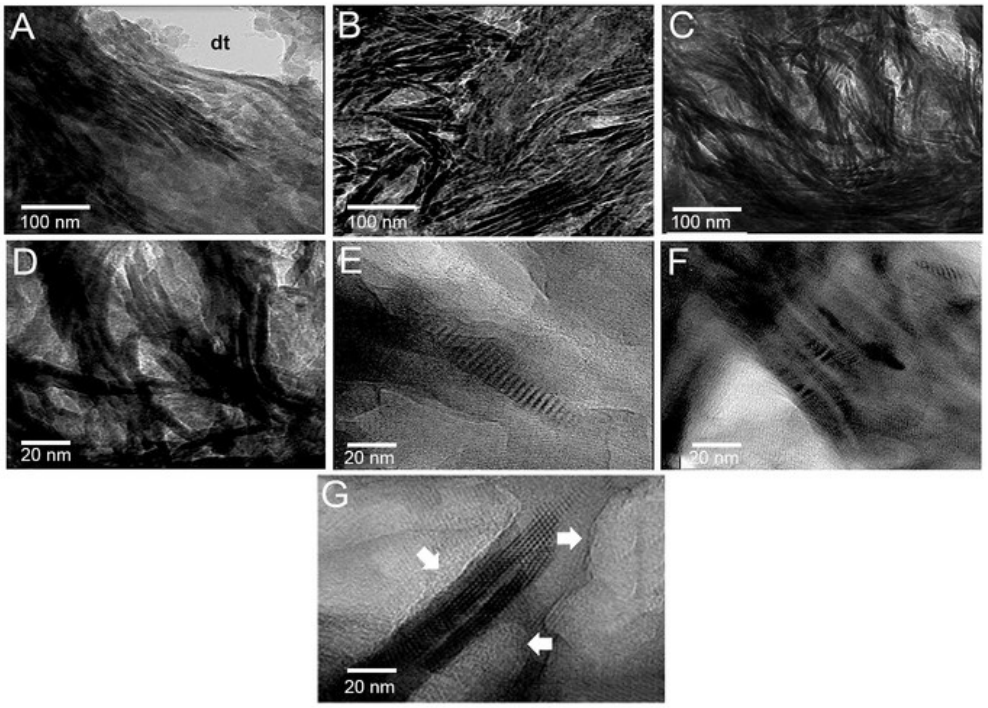

TEM image of (A-B) control specimen demonstrating the continuous presence of collagen fibers near the dentin tubular surface (dt), (C) TEM images show area of aggregated and bundles of collagen in HIFU 10 s specimens; (D) TEM images show area of aggregated and bundles of collagen in 20 s specimens (E) High magnification TEM taken from the more electron-dense regions of the HIFU 10 s specimens showing intact cross-banding patterns with parallel arrangement. (F) High magnification TEM from HIFU 20 s specimens with the intertubular collagen fibrils also revealing intact cross-banding patterns; (G) The white arrows indicated overlap collagen zones identified in the fibril at 5 nm supporting presence of intrafibrillar hydroxyapatite.

58x42mm (300 x 300 DPI)

View Article Online
DOI: 10.1039/D1BM00555C

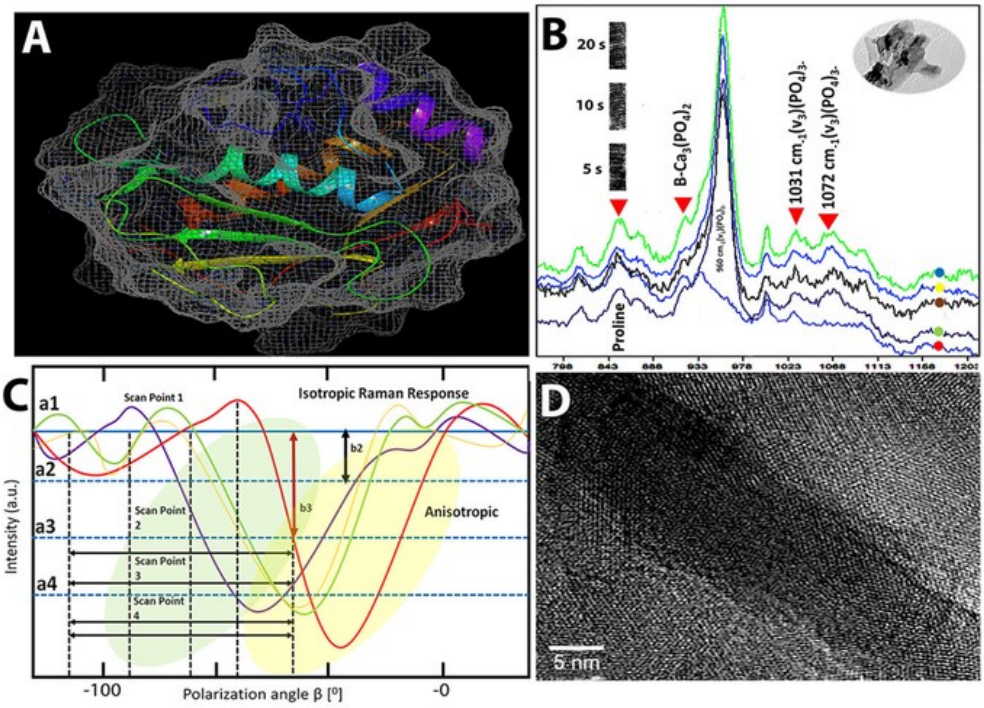

(A) 3D molecular simulation of MMP-2 attachment on collagen Type I; (B) Single Point Raman spectra recorded in the region of dentin in different experimental specimens where the P O bond at 960 cm−1 of the mineral component is well represented in the HIFU treated specimens; (C) Collagen orientation map visualization of demineralized control (red curve), HIFU 20 s (green curve), HIFU 10 s (golden curve) and HIFU 5 s (purple) specimens; (D) Selected high magnification TEM image of HIFU 20 secs treated dentin specimen; a>mean intensity; b>amplitude.

58x42mm (300 x 300 DPI)

View Article Online
DOI: 10.1039/D1BM00555C

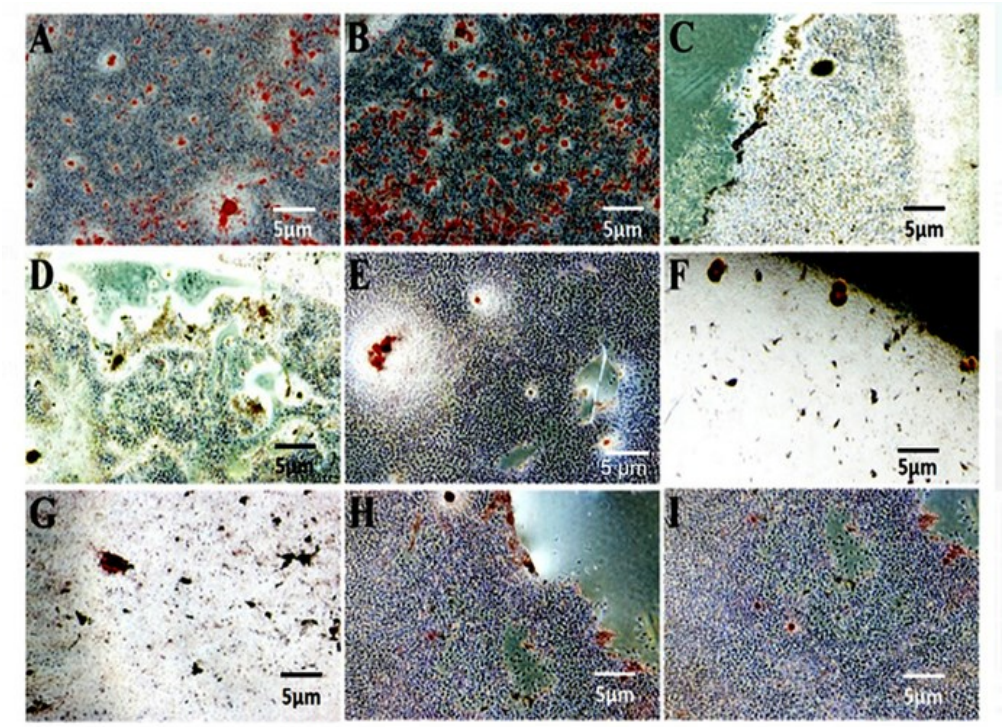

Control and HIFU treated hDPCs were able to adhere to the plastic of petri dishes, proliferated, and formed red nodules in (A-B) control, and (C-E) HIFU 5 secs specimens providing evidence that these cells maintain normal characteristic after 14 days. Alazarin Red-S staining was also observed in cells exposed to (F-G) HIFU 10 secs specimens (B), also showing calcium deposition in (H-I) 20 secs HIFU treated specimens with proliferation media after 14 days. Scale bar: 5 µm.

58x42mm (300 x 300 DPI)

View Article Online
DOI: 10.1039/D1BM00555C

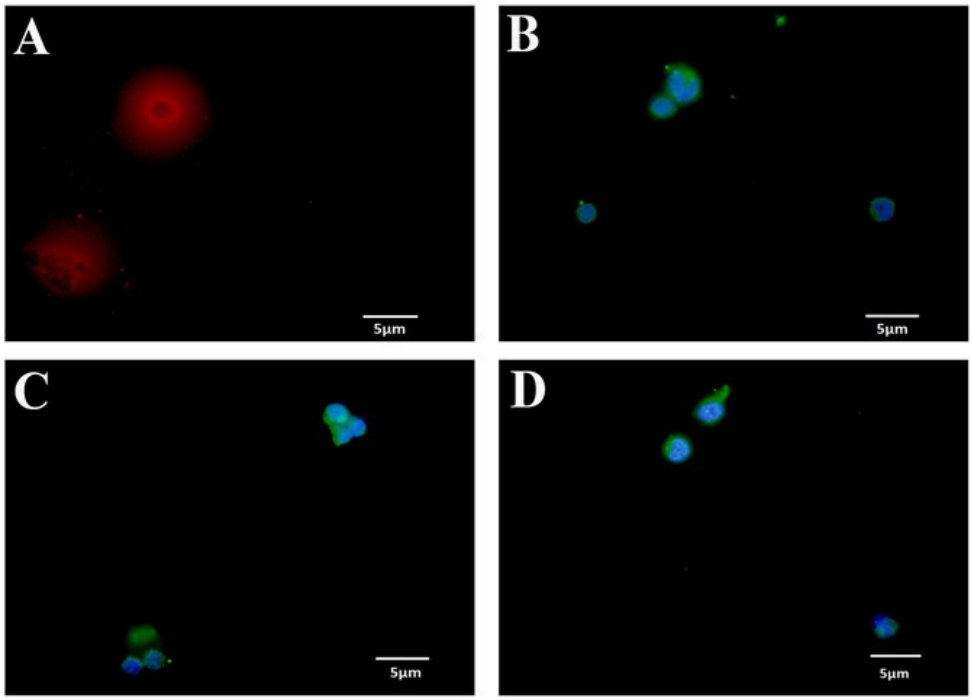

Human peripheral blood mononuclear cell line, SC (CRL-9855 #LOT: 61834527) added with interferon gamma (IFN γ-; 20ng/ml) with the M1 and M2 polarization. CD36+ and CD163 were analysed, and no counter stains of nuclei were used for this experiment. CD80+ and CD 163+ distinguish between macrophage phenotypes. Confocal images of immuno fluorescence staining in (A) Control, (B) 5 secs, (C) 10 secs, (D) 20 secs HIFU treated specimens.

58x42mm (300 x 300 DPI)

View Article Online
DOI: 10.1039/D1BM00555C

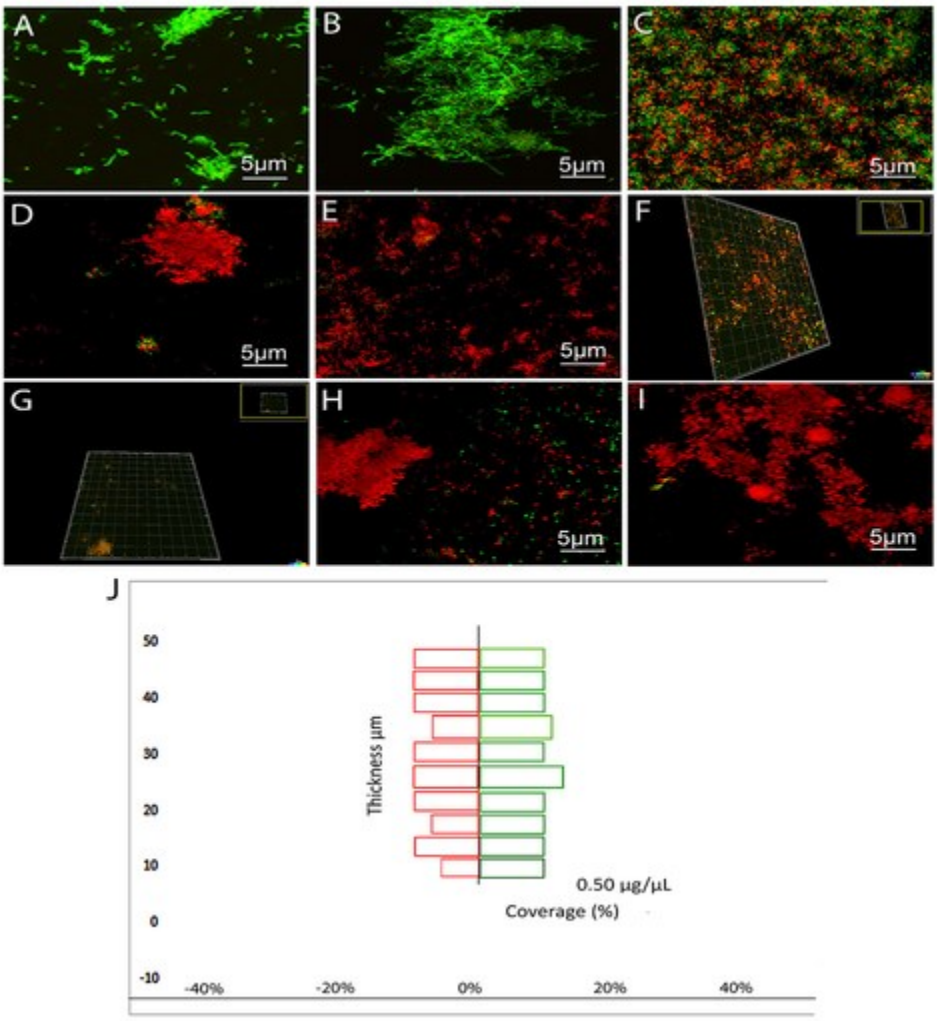

Representative CLSM images of S. mutans grown on dentin discs (A). The control specimens with no treatment effect showing green densely clustered colonies with almost no areas of dead cells after 7 days (B). (C) 5 secs HIFU treated dentin specimens with S mutans biofilm showing areas of dead and minimal vital bacterial colonies; (D-E) 10 secs HIFU treated specimens appeared dead bacterial colonies with no areas of surviving green stained bacteria, indicating no survivability. (F) Three-dimensional reconstruction of the S. mutans biofilms treated with 10 secs HIFU treatment as the ratio of extracellular polysaccharide (EPS) to S. mutans were performed with Imaris 8.0.0. Results were averaged from at least three randomly selected positions. (G) Three-dimensional reconstruction of the S. mutans biofilms treated with 20 secs HIFU treatment as the ratio of EPS to S. mutans were performed with Imaris 8.0.0. (H-I) The HIFU 20 secs specimens showed the highest dead cell count ($p<0.05$). (J) Quantification of the amounts of bacteria in each scanned layer of S. mutans biofilm.

41x43mm (300 x 300 DPI)

View Article Online
DOI: 10.1039/D1BM00555C

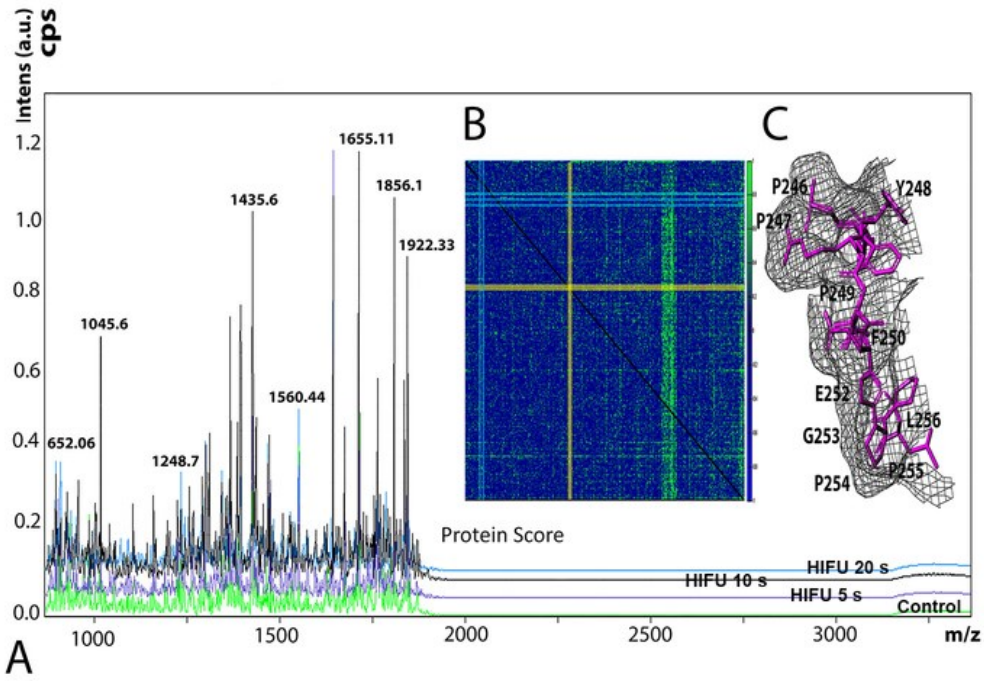

(A) Tandem mass spectrometric analysis of control and HIFU treated specimens. COLTIA1 protein band used for MALDI-MS tryptic peptides showing different ion modes indicating fragmentation species of hydroxyproline and proline; (B) MMP-2 active site mapping with heat map for amino acid occurrences at P', P3 proline and P1' positions identified adding further endorsement to the (C) cleavage sites being tested for MMP-2. The results of MMP-2 concentrations are depicted in the figure with 3D molecular simulation of MMP-2 attachment.

58x40mm (300 x 300 DPI)